Energy detection UWB system based on pulse width modulation

Song Cui, Fuqin Xiong

Department of Electrical and Computer Engineering, Cleveland State University, 2121 Euclid Avenue, Cleveland, OH 44115, USA
E-mail: s.cui99@csuohio.edu

Published in *The Journal of Engineering*; Received on 2nd November 2013; Accepted on 4th March 2014

Abstract: A new energy detection ultra-wideband system based on pulse width modulation is proposed. The bit error rate (BER) performance of this new system is slightly worst than that of a pulse position modulation (PPM) system in additive white Gaussian noise channels. In multipath channels, this system does not suffer from cross-modulation interference as PPM, so it can achieve better BER performance than PPM when cross-modulation interference occurs. In addition, when synchronisation errors occur, this system is more robust than PPM.

1 Introduction

Ultra-wideband (UWB) impulse radio has received more and more attention as a promising technology for many applications, such as short-range and high-speed wireless Internet, covert communications, ground penetrating radar, through-wall image and localisation [1]. In UWB systems, the data are carried by sub-nanosecond pulses and each of these short pulses will generate a large number of multipath components in multipath channels. These multipath components have fine time resolution, so they can be resolved and combined in a Rake receiver [2]. However, the Rake receiver needs a large number of fingers to capture enough signal energy to demodulate the received signals, so this leads to a very complex structure of the receiver and greatly increase the computational burden of channel estimation [2, 3]. In a Rake receiver, each finger includes a correlator and these correlators need extremely accurate synchronisation to align the received signals with the template signals to perform correlation. The acceptable synchronisation error is much smaller than one pulse duration, and a small synchronisation error can severely degrade the system performance [3].

Non-coherent technologies have been developed to avoid the challenges in Rake receivers. Energy detection (ED) has been a conventional non-coherent technology in the communication field for many years. In recent years, ED is applied to UWB systems for on-off keying (OOK) [4–7] and pulse position modulation (PPM) systems [5, 6, 8]. Although ED is a sub-optimal technology, it has many advantages. Its receiver structure is very simple and channel estimation is not required. In addition, ED does not need as accurate synchronisation as a Rake receiver because ED does not use correlators. Now, ED is attracting more and more researchers in the field of UWB.

In this paper, a new ED receiver based on pulse width modulation (PWM) is proposed. Although the popular modulation methods in UWB are PPM and pulse amplitude modulation, PWM has been proved to be a suitable scheme for UWB systems [9]. The receiver in [9] uses a Rake receiver, so we develop the ED receiver in this paper. The bit error rate (BER) performance of this new ED PWM system is slightly worst than that of an ED PPM system in additive white Gaussian noise (AWGN) channels. However, the BER performance of PWM can surpass that of PPM in multipath channels since PWM does not suffer cross-modulation interference (CMI) as PPM. In addition, PWM is more robust to synchronisation errors than PPM, and the BER performance of PWM can be better than PPM when synchronisation errors occur.

The left of this paper is organised as follows. Section 2 introduces the system model. Section 3 analyses the system performance in AWGN channel. Section 4 analyses the system performance in multipath channel. Section 5 analyses the system performance in the presence of synchronisation errors. In Section 6, the numerical results are analysed. Section 7 is the conclusion of this paper.

2 System model

2.1 System model of PWM

In a PWM system, the modulation is achieved by transmitting pulses with different widths to denote bit 0 or 1. The model of the transmitter in [9] is used here. However, we only research the case of single-user communication, and a bit is assumed to transmit only once. Therefore the equation of the transmitter in [9] is simplified to

$$s_{\mathrm{PWM}}(t) = \sum_j \sqrt{E_{\mathrm{p}}} p_{\mathrm{b}_j}(t - \mathrm{j}T_{\mathrm{f}}) \tag{1}$$

where T_{f} denotes the frame period and $p_{\mathrm{b}_j}(t)$ denotes the pulse waveform for jth transmitted data bit b_j. The data bit has a binary value of either 0 or 1. When bit 0 or 1 is transmitted, the transmitted pulse waveform is $p_0(t)$ or $p_1(t)$, respectively, where $p_0(t)$ and $p_1(t)$ are amplitude-normalised pulse waveforms with different widths. The pulse energy is adjusted by E_{p} and the energies of $p_0(t)$ and $p_1(t)$ are different. Therefore we define the energies of the pulses for bits 0 and 1, E_0 and E_1, by $E_i = E_{\mathrm{p}} \int_{-T_{\mathrm{p}_i}/2}^{T_{\mathrm{p}_i}/2} [p_i(t)]^2 \, \mathrm{d}t$, $(i = 0, 1)$, where T_{p_i} is the pulse width. The ratio E_0/E_1 depends on which pulse waveforms are chosen [9]. In this paper, we use the second-order derivative of the Gaussian pulse [10]

$$p(t) = (1 - 4\pi t^2/\alpha_i^2) \exp(-2\pi t^2/\alpha_i^2) \tag{2}$$

where α_i is the shape factor. The pulse width T_{p_i} is set to $2.4\alpha_i$ and the detailed method to choose the pulse width for a specific α_i value can be found in [10]. After the second-order derivative of the Gaussian pulse is chosen, the modulation is achieved by using different α_i values for bits 0 and 1. Increasing α_i will increase T_{p_i} and thus decrease the bandwidth. We choose $\alpha_1 = 2\alpha_0$ to achieve modulation, where α_1 and α_0 are the shape factors for $p_1(t)$ and $p_0(t)$, respectively. Therefore we have $T_{\mathrm{p}_1} = 2T_{\mathrm{p}_0}$, where T_{p_1} and T_{p_0} denote the width of $p_1(t)$ and $p_0(t)$, respectively. Based on these assignments, the relationship between E_0 and E_1 is

$$E_0 = 0.5E_1 \tag{3}$$

doi: 10.1049/joe.2013.0172

A simple proof of (3) is given as follows: the values of E_0 and E_1 are $E_0 = E_p \int_{-1.2\alpha_0}^{1.2\alpha_0} (1 - 4\pi t^2/\alpha_0^2)^2 \, e^{-4\pi t^2/\alpha_0^2} \, dt$ and $E_1 = E_p \int_{-1.2\alpha_1}^{1.2\alpha_1} (1 - 4\pi t^2/\alpha_1^2)^2 \, e^{-4\pi t^2/\alpha_1^2} \, dt$, respectively. Since $\alpha_1 = 2\alpha_0$, we let $\tau = t/2$. And then it is straightforward to use the new variable τ to convert E_1 to $E_1 = 2E_p \int_{-1.2\alpha_0}^{1.2\alpha_0} (1 - 4\pi\tau^2/\alpha_0^2)^2 \, e^{-4\pi\tau^2/\alpha_0^2} \, d\tau = 2E_0$.

The design idea of the receiver originates from the spectral characteristics of the Gaussian pulse. The Fourier transform X_f and centre frequency f_c of the kth-order derivative of the Gaussian pulse are [10]

$$X_f \propto f^k \exp(-\pi f^2 \alpha_i^2/2) \tag{4}$$

$$f_c = \sqrt{k}/(\alpha_i \sqrt{\pi}) \tag{5}$$

where f is the frequency. Using (4), the spectra of $p_0(t)$ and $p_1(t)$ are plotted in Fig. 1. The bandwidth of $p_0(t)$ is almost twice that of $p_1(t)$. The centre frequency of $p_0(t)$ is f_{c0}. Two ideal filters, Filters 1 and 2, are also shown in Fig. 1. The passband of Filter 1 is [0, f_{c0}] and that of Filter 2 is [f_{c0}, $2f_{c0}$]. When $p_0(t)$ is transmitted, both Filters 1 and 2 pass about half of its energy. If we subtract the signal energies captured by Filters 1 and 2, the result is ~ 0. When $p_1(t)$ is transmitted, Filter 1 passes almost all of the energy of $p_1(t)$, but Filter 2 rejects the energy of $p_1(t)$. Therefore, if we subtract the energies, the result is $\sim E_1$. We can determine the transmitted bit is 0 or 1 by measuring the difference of signal energies captured by the two filters. This inspires us to design the receiver as in Fig. 2. To make sure that our design idea of the receiver is based on strict theoretical support rather than direct observable results, we use MAPLE software to perform numerical calculation to obtain the following equations

$$E_{01} - E_{02} \simeq 0 \tag{6}$$

$$E_{01} + E_{02} \simeq E_0 \tag{7}$$

$$E_{11} - E_{12} \simeq E_1 \tag{8}$$

$$E_{11} + E_{12} \simeq E_1 \tag{9}$$

where E_{01}, E_{02}, E_{11} and E_{12} denote the signal energies captured by the two filters. The first subscript denotes the transmitted bit is 0 or 1 and the second subscript means Filter 1 or 2. The detailed procedure to obtain these equations is given in Appendix. Equations (6) and (8) show the adequate theory support for our design idea.

The receiver in Fig. 2 has two branches, and each branch is a conventional ED receiver. The only difference between the two branches is the passbands of the filters. The passbands of Filters 1 and 2 are like that in Fig. 1. The signal arriving at the receiver is denoted by $s(t)$, the AWGN is denoted by $n(t)$, and the sum of $s(t)$ and $n(t)$ is denoted by $r(t)$. The integration interval $T \le T_f$. The decision statistic is given by $Z = Z_1 - Z_2$, where Z_1 and Z_2 are the outputs of branches 1 and 2, respectively. Finally, Z is compared with threshold γ to determine the transmitted bit. If $Z \ge \gamma$, the transmitted bit is 1, otherwise it is 0.

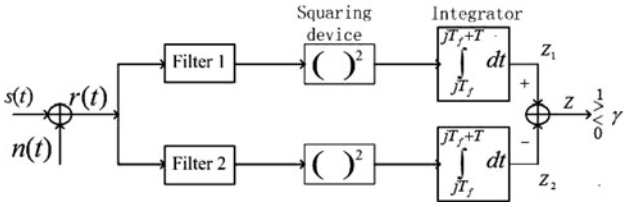

Fig. 2 *Receiver structure of an ED PWM system*

We will compare the performance of this new system with the existing ones in the following, and the models of these systems are simply stated as follows: the OOK system does not transmit a signal when data are 0, so it has difficulty to achieve synchronisation, especially when a stream of zeros is transmitted [11]. Therefore we only compare PPM with our new system in this paper. In Section 2.2, the system model of PPM is depicted.

2.2 System model of PPM

The transmitted signal of a PPM system is [12]

$$s(t)_{PPM} = \sum_j \sqrt{E_p} p(t - jT_f - \delta b_j) \tag{10}$$

where δ is called the modulation index and the pulse shift amount is determined by δb_j. The frame period is denoted by T_f, $p(t)$ is the pulse waveform with normalised-energy and E_p denotes signal energy. The receiver of an ED PPM system includes a conventional ED receiver, and the decision statistic Z is obtained as [13]

$$Z = Z_1 - Z_2 = \int_{jT_f}^{jT_f+T} r^2(t)\,dt - \int_{jT_f+\delta}^{jT_f+\delta+T} r^2(t)\,dt \tag{11}$$

where $T \le \delta$ denotes the length of integration interval. The decision threshold of PPM is $\gamma = 0$. If $Z \ge \gamma = 0$, the transmitted bit is 0, otherwise it is 1.

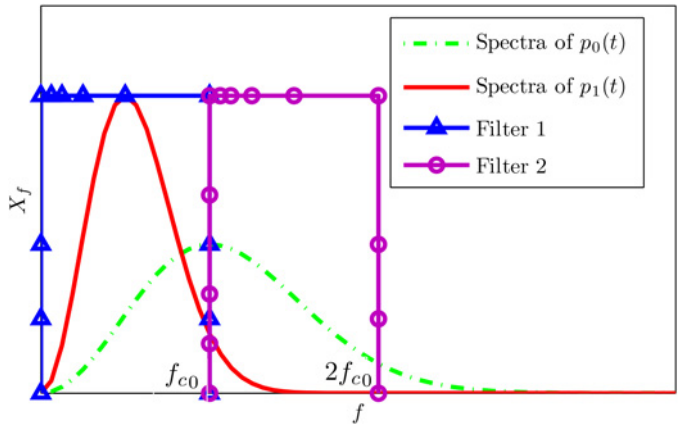

Fig. 1 *Spectral curves of $p_0(t)$ and $p_1(t)$ and the passbands of Filters 1 and 2*

3 BER performance in AWGN channels

3.1 PWM performance in AWGN channels

In Fig. 2, the outputs of conventional energy detectors, Z_1 and Z_2, are chi-square variables with approximately a degree of $2TW$ [14], where W denotes the bandwidth of the filters and T denotes the integration time. When the value of $2TW$ is large, the chi-square variable is approximated as a Gaussian variable. This popular method is called Gaussian approximation in ED communication systems [5, 13, 15–17]. The mean value and variance of this Gaussian variable are [18]

$$\mu = N_0TW + E \tag{12}$$

$$\sigma^2 = N_0^2TW + 2N_0E \tag{13}$$

where μ and σ^2 are the mean value and variance, and $N_0/2$ denotes the double-sided power spectral density of AWGN. The signal energy captured by the filter is denoted by E. If the spectrum of the signal does not fall in the passband of filter, then $E = 0$. In Fig. 2, when bit 0 is transmitted, the signal energy almost distributes equally in the passbands of Filters 1 and 2. The probability density functions (pdfs) of Z_1 and Z_2 are $Z_1 \sim N(N_0TW + E_{01},\ N_0^2TW + 2N_0E_{01})$ and $Z_2 \sim N(N_0TW + E_{02},\ N_0^2TW + 2N_0E_{02})$. Since $Z = Z_1 - Z_2$, we have $Z \sim N(E_{01} - E_{02},\ 2N_0^2TW + 2N_0(E_{01} + E_{02}))$. Using (6) and (7), the pdf of Z is

$$H_0{:}Z \sim N(0,\ 2N_0^2TW + 2N_0E_0) \tag{14}$$

When bit 1 is transmitted, the signal energy almost passes through Filter 1 entirely. The pdf of Z_1 and Z_2 can be expressed as $Z_1 \sim N(N_0TW + E_{11},\ N_0^2TW + 2N_0E_{11})$ and $Z_2 \sim N(N_0TW + E_{12},\ N_0^2TW + 2N_0E_{12})$. The pdf of Z is $Z \sim N(E_{11} - E_{12},\ 2N_0^2TW + 2N_0(E_{11} + E_{12}))$. Using (8) and (9), the pdf of Z becomes

$$H_1{:}Z \sim N(E_1,\ 2N_0^2TW + 2N_0E_1) \tag{15}$$

Since E_0 and E_1 have different values, we will denote them using average bit energy E_b. Assuming bits 0 and 1 are randomly transmitted at the same probability, we obtain $E_b = (1/2)(E_0 + E_1)$ [5, 6]. From (3), we have $E_0 = 0.5E_1$, so E_0 and E_1 can be expressed as

$$E_0 = \frac{2}{3}E_b \tag{16}$$

$$E_1 = \frac{4}{3}E_b \tag{17}$$

Substituting (16) and (17) into (14) and (15), respectively, we obtain

$$H_0{:}Z \sim N\left(0,\ 2N_0^2TW + \frac{4}{3}N_0E_b\right) \tag{18}$$

$$H_1{:}Z \sim N\left(\frac{4}{3}E_b,\ 2N_0^2TW + \frac{8}{3}N_0E_b\right) \tag{19}$$

We follow the method in [15] to derive BER using (18) and (19). Firstly, we calculate the BER when bits 0 and 1 are transmitted as follows

$$P_0 = \int_\gamma^\infty f_0(x)\,\mathrm{d}x = \int_\gamma^\infty \frac{1}{\sqrt{2\pi}\sigma_0} \mathrm{e}^{-\left((x-\mu_0)^2/2\sigma_0^2\right)}\,\mathrm{d}x \tag{20}$$

$$P_1 = \int_{-\infty}^\gamma f_1(x)\,\mathrm{d}x = \int_{-\infty}^\gamma \frac{1}{\sqrt{2\pi}\sigma_1} \mathrm{e}^{-\left((x-\mu_1)^2/2\sigma_1^2\right)}\,\mathrm{d}x \tag{21}$$

where $f_0(x)$ and $f_1(x)$ denote the pdfs of Z when bits 0 and 1 are transmitted, respectively, and γ denotes the decision threshold. From (18) and (19), it is straightforward to obtain $\mu_0 = 0$, $\sigma_0^2 = 2N_0^2TW + \frac{4}{3}N_0E_b$, $\mu_1 = (4/3)E_b$, $\sigma_1^2 = 2N_0^2TW + \frac{8}{3}N_0E_b$. Substituting these parameter values into (20) and (21), and then expressing P_0 and P_1 in terms of the complementary error function $Q(\cdot)$, we obtain

$$P_0 = Q\left(\gamma/\sqrt{2N_0^2TW + \frac{4}{3}N_0E_b}\right) \tag{22}$$

$$P_1 = Q\left(\left(\frac{4}{3}E_b - \gamma\right)/\sqrt{2N_0^2TW + \frac{8}{3}N_0E_b}\right) \tag{23}$$

The optimal threshold is obtained by setting $P_0 = P_1$ [5, 15, 17], and then we have

$$\frac{\gamma}{\sqrt{2N_0^2TW + \frac{4}{3}N_0E_b}} = \frac{((4/3)E_b - \gamma)}{\sqrt{2N_0^2TW + (8/3)N_0E_b}} \tag{24}$$

Solving (24), the optimal threshold is

$$\gamma = \frac{((4/3)E_b)\sqrt{2N_0^2TW + (4/3)N_0E_b}}{\sqrt{2N_0^2TW + (8/3)N_0E_b} + \sqrt{2N_0^2TW + (4/3)N_0E_b}} \tag{25}$$

The total BER is $P_e = 0.5(P_0 + P_1)$. Since $P_0 = P_1$, we have $P_e = P_0$. Substituting (25) into (22), the total BER of PWM in AWGN channels is

$$P_e = Q\left(\frac{(4/3)(E_b/N_0)}{\sqrt{2TW + (8/3)(E_b/N_0)} + \sqrt{2TW + (4/3)(E_b/N_0)}}\right) \tag{26}$$

3.2 PPM performance in AWGN channels

The BER equation of ED PPM has been derived in [5], and its expression is as follows

$$P_e = Q\left(\frac{E_b/N_0}{\sqrt{2TW + 2E_b/N_0}}\right) \tag{27}$$

4 BER performance in multipath channels

In this section, the BER performances of PPM and PWM in multipath channels are researched. The IEEE 802.15.4a channel model [19] is used in this paper. The signal convolves with the channel impulse response in multipath channels and becomes

$$r(t) = s(t) \otimes h(t) + n(t) \tag{28}$$

where $h(t)$ denotes the channel impulse response, $n(t)$ is AWGN and the convolution operation is denoted by $\otimes$.

4.1 PPM performance in multipath channels

The BER performance of PPM in multipath channels was analysed in our previous publication [17], so we briefly summarise it as follows. Fig. 3 shows the frame structures of PPM in multipath channels. In Fig. 3, δ denotes modulation index, T_0 and T_1 are the time intervals reserved for multipath components of bits 0 and 1, respectively. The relationship of the above three parameters is $\delta = T_0 = T_1$. The value of δ must be designed appropriately. A too large value will waste the transmission time and reduce the data rate. However, if it is less than the maximum channel spread D,

doi: 10.1049/joe.2013.0172

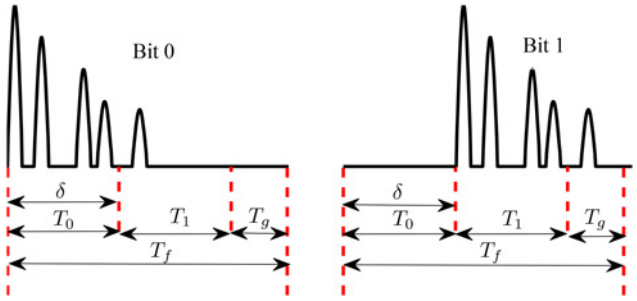

Fig. 3 *PPM frame structures in multipath channels*

the CMI will occur [13, 16, 17, 20]. In fact, it is difficult to guarantee that the value of δ is always appropriate, so the effect of CMI on system performance cannot be neglected. When CMI occurs, the system performance will degrade considerably. Even increasing the transmitting power will not improve the performance because of the proportional increase of interference [17, 20]. Synchronisation error is assumed to be 0 in analysis. When δ is less than the maximum channel spread D, some multipath components of bit 0 extend into the interval T_1 and cause CMI. However, the multipath components of bit 1 do not cause CMI and some of them just extend into the guard interval T_g, which is used to prevent inter-frame interference (IFI). The frame period is $T_f = T_0 + T_1 + T_g$. To achieve as high a data rate as possible and prevent IFI simultaneously, the frame period is set to $T_f = \delta + D$ [13, 17].

The BER of PPM in multipath channels is derived in [17]

$$P_e = \frac{1}{2}Q\left(\frac{(\beta_a - \beta_b)(E_b/N_0)}{\sqrt{2TW + 2(\beta_a + \beta_b)(E_b/N_0)}}\right) + \frac{1}{2}Q\left(\frac{\beta_a(E_b/N_0)}{\sqrt{2TW + 2\beta_a(E_b/N_0)}}\right) \tag{29}$$

where β_a and β_b are defined as follows. When bit 0 is transmitted, $\beta_a = E_{T_0}/E_b$ and $\beta_b = E_{T_1}/E_b$. The two variables, E_{T_0} and E_{T_1}, denote the captured signal energies in the integration intervals T_0 and T_1, respectively. Under this conversion, E_{T_0} and E_{T_1} are expressed as $\beta_a E_b$ and $\beta_b E_b$, respectively. The values of β_a and β_b are in the range [0, 1]. When bit 1 is transmitted, $E_{T_0} = 0$ and $E_{T_1} = \beta_a E_b$. When there is no CMI, $\beta_a = 1$ and $\beta_b = 0$, (29) reduces to (27).

4.2 PWM performance in multipath channels

Fig. 4 is the frame structure of PWM in multipath channels. CMI does not occur as it does in PPM systems. To compare PWM with PPM under the same energy capture condition, the integration interval T_0 of PWM has the same length as the T_0 of PPM. In addition, synchronisation is assumed to be perfect as in PPM. The guard interval is T_g, and the frame period is set to $T_f = T_0 + T_g = D$. This will achieve the maximum data rate and prevent IFI simultaneously. This frame structure is applied to both bits 0 and 1. We assume λ denotes the ratio of the captured signal energy in interval T_0 to the total signal energy at each branch. When bit 0 is transmitted, the signal energy distributes almost equally to two branches, that is $E_{01} = E_{02} = E_b/3$. Therefore the captured signal energy E_{T_0} in two branches are all $\lambda E_b/3$, and the resultant pdf of Z is

$$H_0: Z \sim N\left(0,\ 2N_0^2TW + N_0\lambda\frac{4}{3}E_b\right) \tag{30}$$

When bit 1 is transmitted, the signal energy almost entirely distributes to Branch 1, and the signal energy of Branch 2 is ~0. Therefore we have $E_{11} = 4\lambda E_b/3$ and $E_{12} = 0$. The pdf of Z is

$$H_1: Z \sim N\left(\lambda\frac{4}{3}E_b,\ 2N_0^2TW + N_0\lambda\frac{8}{3}E_b\right) \tag{31}$$

Using (20) and (21), and following the method in Section 3.1, we obtain the decision threshold γ and BER as follows

$$\gamma = \frac{((4/3)\lambda E_b)\sqrt{2N_0^2TW + (4/3)N_0\lambda E_b}}{\sqrt{2N_0^2TW + (8/3)N_0\lambda E_b} + \sqrt{2N_0^2TW + (4/3)N_0\lambda E_b}} \tag{32}$$

$$P_e = Q\left(\frac{(4/3)\lambda(E_b/N_0)}{\sqrt{2TW + (8/3)\lambda(E_b/N_0)} + \sqrt{2TW + (4/3)\lambda(E_b/N_0)}}\right) \tag{33}$$

where γ is not a constant and it is changed by the captured energy in interval T_0. When $T_0 = D$, the integrators capture all signal energy and then $\lambda = 1$. Equations (32) and (33) reduce to (25) and (26), respectively.

5 BER performance in the presence of synchronisation errors

5.1 PPM performance in the presence of synchronisation errors

The BER performance of PPM in the presence of synchronisation errors is analysed in our publication [17]. A brief summary is as follows. In Fig. 5, the PPM frame structures in the presence of synchronisation errors ε are shown. Since only the effect of synchronisation errors is analysed, so the modulation index is set to $\delta = D = T_0 = T_1$ to avoid CMI. The BER performances of PPM is analysed in the range $\varepsilon \in [0, D/2]$. The frame length is set to $T_f = 2D + T_g$, where the value of the guard interval T_g is set to $D/2$, the

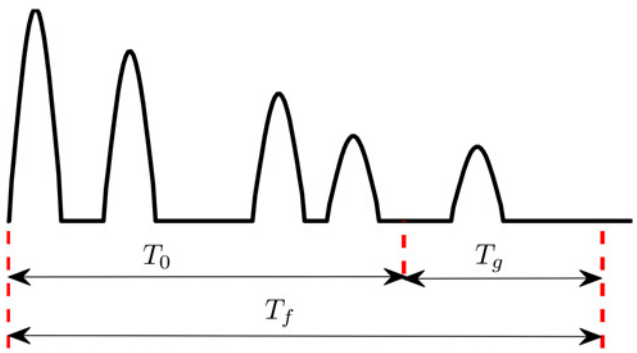

Fig. 4 *PWM frame structures in multipath channels*

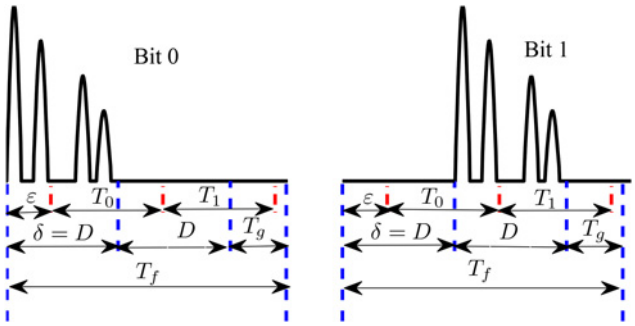

Fig. 5 *PPM frame structures in the presence of synchronisation errors*

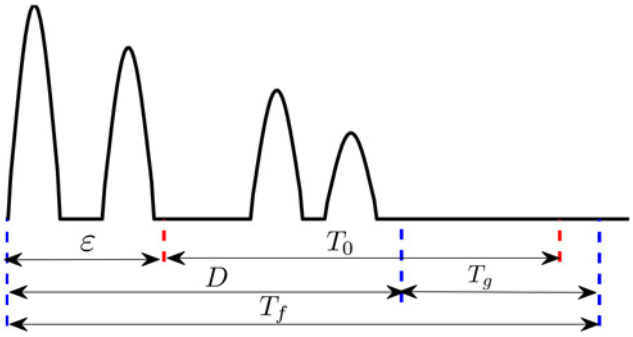

Fig. 6 *PWM frame structure in the presence of synchronisation errors*

maximum synchronisation error used in analysis. Under this frame length design, IFI is effectively avoided.

The BER of PPM in the presence of synchronisation errors is [17]

$$P_e = \frac{1}{2}Q\left(\frac{\eta E_b/N_0}{\sqrt{2TW + 2\eta E_b/N_0}}\right) + \frac{1}{2}Q\left(\frac{(2\eta - 1)E_b/N_0}{\sqrt{2TW + 2E_b/N_0}}\right) \quad (34)$$

where η is defined as follows. When bit 0 is transmitted, $\eta = E_{T_0}/E_b$ and $E_{T_1} = 0$. When bit 1 is transmitted, $\eta = E_{T_1}/E_b$ and $E_{T_0} = (1 - \eta)E_b$.

5.2 PWM performance in the presence of synchronisation errors

Fig. 6 depicts the PWM frame structure in the presence of synchronisation errors ε. The integration interval $T_0 = D$ is the same as that of PPM. The frame length is $T_f = T_g + D$, where $T_g = D/2$ as in Section 5.1. From Fig. 6, the pdfs of Z are

$$H_0: Z \sim N\left(0,\ 2N_0^2TW + \frac{4}{3}N_0\rho E_b\right) \quad (35)$$

$$H_1: Z \sim N\left(\frac{4}{3}\rho E_b,\ 2N_0^2TW + \frac{8}{3}N_0\rho E_b\right) \quad (36)$$

where ρ denotes the ratio of the captured signal energy in T_0 to the total signal energy at each branch. Using (20) and (21), and following the method in Section 3.1, the decision threshold γ and total BER are

$$\gamma = \frac{((4/3)\rho E_b)\sqrt{2N_0^2TW + (4/3)N_0\rho E_b}}{\sqrt{2N_0^2TW + (8/3)N_0\rho E_b} + \sqrt{2N_0^2TW + (4/3)N_0\rho E_b}} \quad (37)$$

$$P_e = Q\left(\frac{(4/3)\rho(E_b/N_0)}{\sqrt{2TW + (8/3)\rho(E_b/N_0)} + \sqrt{2TW + (4/3)\rho(E_b/N_0)}}\right) \quad (38)$$

where γ is also an adaptive threshold. When $\varepsilon = 0$, no synchronisation errors occur and the integrators capture all signal energy. Therefore we have $\rho = 1$ and then (37) and (38) reduce to (25) and (26), respectively.

6 Numerical results and analysis

Fig. 7 shows the BER curves of PWM for different $2TW$ values in AWGN channels. In simulation, the bandwidth of the filters is 3 GHz, the shape factors for bits 0 and 1 are 0.25×10^{-9} and 0.5×10^{-9}, respectively, and the corresponding pulse durations are 0.6 and 1.2 ns. The analytical BER curves are obtained directly from (26). From Fig. 7, it is observed that the simulated and analytical curves match better when $2TW$ is increased. The reason is that the Gaussian approximation is more accurate under large $2TW$ values [15, 17]. After the bandwidth W is chosen, we only can change $2TW$ by changing the integration time T. Therefore the Gaussian approximation is more accurate when T is larger. However, the large T degrades BER performance since the integrator captures more noise energy [17]. After the UWB signal travels through the multipath channel, the large number of multipath

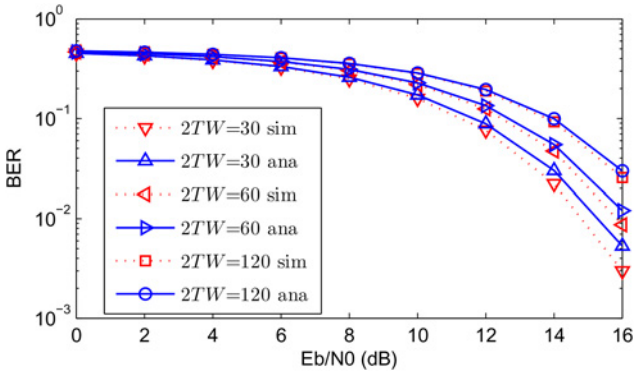

Fig. 7 *BER performance of PWM for different 2TW values in AWGN channels*

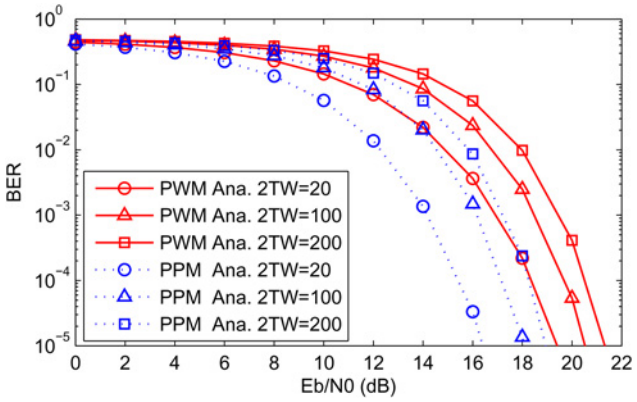

Fig. 8 *Comparison of BER performance of PWM and PPM for different 2TW values*

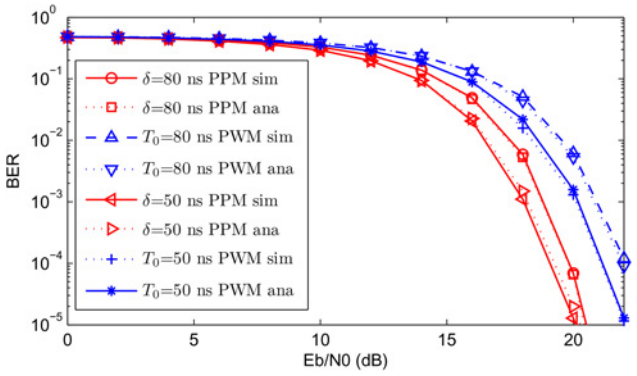

Fig. 9 *Comparison of BER performance of PWM and PPM in multipath channels (δ = 80 and 50 ns)*

doi: 10.1049/joe.2013.0172

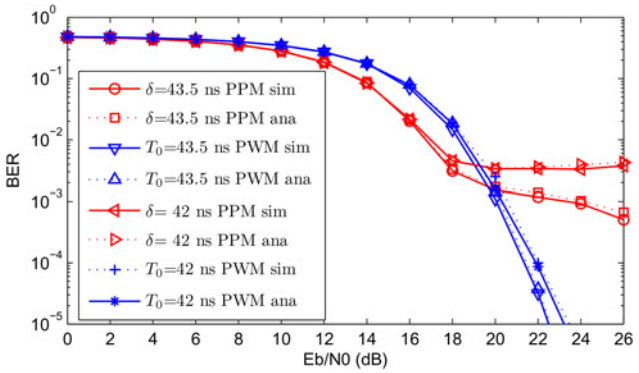

Fig. 10 *Comparison of BER performance of PWM and PPM in multipath channels ($\delta = 43.5$ and 42 ns)*

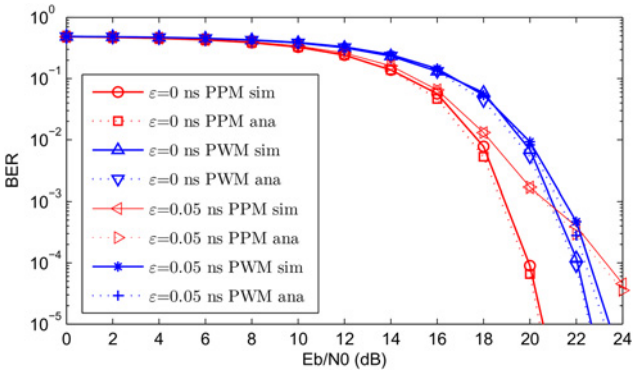

Fig. 11 *Comparison of BER performance of PWM and PPM in the presence of synchronisation errors ($\varepsilon = 0$ and 0.05 ns)*

components cause a very long channel delay. To capture the enough signal energy, the integration interval must be very long and this leads to a very large $2TW$ value.

Fig. 8 shows the analytical BER curves of PWM and PPM for different $2TW$ values. Since (26) has been proved an accurate BER equation for PWM above and (27) was also proved to be accurate for PPM [5], we use analytical BER curves to compare the BER performances of PWM and PPM in AWGN channels. In Fig. 8, When $2TW = 20$, PPM achieves 2.7 dB improvement over PWM at BER = 10^{-3}. When $2TW = 100$ and 200, the improvements are 2.3 and 2.2 dB, respectively. An ED PPM system exhibits better BER performance than an ED PWM system in AWGN channels.

Figs. 9 and 10 show the BER performance comparisons of PWM and PPM in multipath channels. In simulation, the shape factor of the pulses for PPM is 0.5×10^{-9} and the bandwidth of the filter is 3 GHz, the same as PWM. The CM1 model [19] is used in simulation. Synchronisation is perfect, and the maximum channel spread D is truncated to 80 ns. The frame length is designed using the method mentioned in Section 4, so IFI is avoided in simulation. In this paper, $\delta = T_0 = T_1$ for PPM, and the T_0 of PWM equals the T_0 of PPM. In the following, when a value of δ is given, it implies that T_0 and T_1 also have the same value. Therefore we only mention δ in the following. The analytical BER curves of PPM and PWM are obtained directly from (29) and (33), respectively. In these two equations, we need to know the values of parameters β_a, β_b and λ. There is no mathematical formula to calculate the captured energy as a function of the length of the integration interval for IEEE 802.15.4a channel. Therefore we use the statistic method in [17] to obtain values for the above parameters. Firstly, the MATLAB code in [19] is used to generate realisations of the channel impulse response $h(t)$. Then, we calculate the ratio of energy in a specific time interval to the total energy of a channel realisation to obtain the values for these parameters. These values are substituted into (29) and (33) to achieve the analytical BER. Both the simulated and the analytical BER are obtained by averaging over 100 channel realisations. In Fig. 9, when $\delta = 80$ ns, no CMI occurs and PPM achieves better BER performance than PWM. The improvement is ~2.1 dB at BER = 10^{-3}. When $\delta =$ 50 ns, PPM still achieves better BER performance than PWM in spite of the slight CMI and the improvement is ~2 dB at BER = 10^{-3}.

However, we can see from Fig. 9 that the performances of PWM and PPM are both improved compared with when $\delta = 80$ ns. The reason is that the multipath components existing in the time interval between 50 and 80 ns include low signal energy and the integrators capture more noise energy than signal energy in this interval. In Fig. 10, when $\delta = 43.5$ ns, PWM achieves better BER performance than PPM and the improvement is ~4 dB at BER = 10^{-3}. When $\delta = 42$ ns, PWM requires an increase of E_b/N_0 ~0.2 dB to maintain

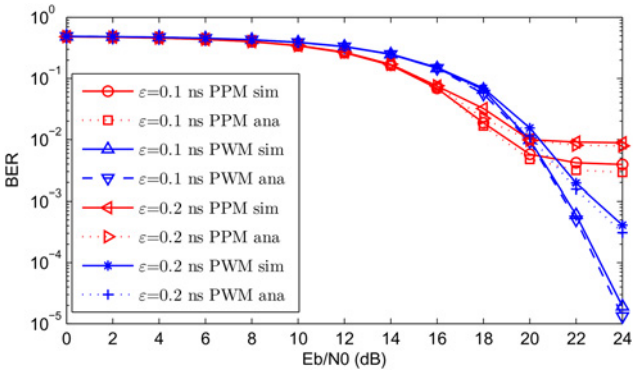

Fig. 12 *Comparison of BER performance of PWM and PPM in the presence of synchronisation errors ($\varepsilon = 0.1$ and 0.2 ns)*

BER = 10^{-3}. However, PPM cannot achieve this BER level and exhibits a BER floor. The BER performance of PPM cannot be improved by increasing the transmitted power because of the proportional increase of CMI [17, 20]. Unlike PPM, however, PWM still achieves a good BER performance when the signal transmitting power is increased.

Figs. 11 and 12 are comparisons of BER performance when synchronisation errors occur. In simulation, the modulation index δ is set to the maximum channel spread $D = 80$ ns, so no CMI occurs in simulation. The frame structure is designed by following the method mentioned in Section 5, so IFI is avoided in simulation. The analytical BER curves are obtained directly from (34) and (38), and the values for parameters η and ρ in (34) and (38) are obtained by using the statistic method similar to the one described above. Both the simulated and analytical BERs are obtained by averaging over 100 channel realisations. In Fig. 11, when $\varepsilon = 0$ ns, no synchronisation error occurs, and PPM achieves better BER performance than PWM. The improvement is ~2.1 dB at BER = 10^{-3}. When $\varepsilon = 0.05$ ns, PPM still achieves ~0.5 dB improvement at BER = 10^{-3}. However, there is a crossing point between the BER curves of PWM and PPM. The BER performance of PWM actually has surpassed PPM if we compare them using better BER values. In Fig. 12, when $\varepsilon = 0.1$ and 0.2 ns, the BER curves of PPM exhibit BER floors because of a severe synchronsation error, but PWM still achieves a good BER. When we compare these synchronisation error values to the maximum channel delay, they are really very small. Even it is still small when we compare them with the duration of a single pulse. Under so small synchronisation errors, PPM has been degraded severely. However, PWM still can achieve good BER performance. Therefore the robustness of PWM is very significant.

The reason the BER performance of PWM is better than PPM in the presence of CMI or synchronisation errors can be explained as follows: in a PPM system, modulation is achieved by shifting the pulse position, and the orthogonality of the signals is achieved in time domain. When CMI or synchronisation errors occur, this orthogonality is easily destroyed [17]. And this results in the energy cancellation between T_0 and T_1, thereby the euclidean distance is reduced dramatically and the BER performance is severely degraded. In a PWM system, when bit 0 is transmitted, the mean values in (30) and (35) are always 0. The euclidean distance is not affected by small T_0 values or synchronisation errors when bit 0 is transmitted. When bit 1 is transmitted, although the mean values in (31) and (36) are reduced, but the phenomena of energy cancellation does not occur in a PWM system.

7 Conclusion

A new ED UWB system based on pulse width modulation is proposed in this paper. The BER performance of this new system is compared with PPM in AWGN channels, multipath channels and in the presence of synchronisation errors. In AWGN channels, the BER performance of PPM is slightly better than PWM. However, in multipath channels, PPM suffers from CMI if the integration interval is shorter than maximum channel spread. This causes the degradation of BER performance of PPM, so the BER performance of PWM can surpass that of PPM in multipath channels. In addition, when synchronisation errors occur, PWM is more robust and achieves better BER performance than PPM. If we choose PWM other than PPM, it will lower the requirement of synchronisation accuracy and we can choose cheap synchroniser to reduce the cost.

8 References

[1] Yang L., Giannakis G.B.: 'Ultra-wideband communications: an idea whose time has come', *IEEE Signal Process. Mag.*, 2004, **21**, (6), pp. 26–54

[2] Carbonelli C., Mengali U.: 'M-PPM noncoherent receivers for UWB applications', *IEEE Trans. Wirel. Commun.*, 2006, **5**, (8), pp. 2285–2294

[3] He N., Tepedelenlioglu C.: 'Performance analysis of non-coherent UWB receivers at different synchronization levels', *IEEE Trans. Wirel. Commun.*, 2006, **5**, (6), pp. 1266–1273

[4] Paquelet S., Aubert L.M.: 'An energy adaptive demodulation for high data rates with impulse radio'. IEEE Radio and Wireless Conf., Atlanta, USA, September 2004, pp. 323–326

[5] Dubouloz S., Denis B., de Rivaz S., Ouvry L.: 'Performance analysis of LDR UWB non-coherent receivers in multipath environments'. IEEE Int. Conf. Ultra-Wideband, Zurich, Switzerland, September 2005, pp. 491–496

[6] Witrisal K., Leus G., Janssen G., *ET AL.*: 'Noncoherent ultra-wideband systems', *IEEE Signal Process. Mag.*, 2009, **26**, (4), pp. 48–66

[7] Mu D., Qiu Z.: 'Weighted non-coherent energy detection receiver for UWB OOK system'. IEEE the Ninth Int. Conf. Signal Processing, Beijing, China, October 2008, pp. 1846–1849

[8] Amico A., Mengali U., Arias-de-reyna E.: 'Energy-detection UWB receivers with multiple energy measurements', *IEEE Trans. Wirel. Commun.*, 2007, **6**, (7), pp. 2652–2659

[9] Wang F., Xu C., Ji X., Zhang Y.: 'Performance analysis of time-hopping pulse width modulation impulse radio'. The Fourth Int. Conf. Wireless Communication, Networking and Mobile Computing, Dalian, China, October 2008, pp. 1–5

[10] Benedetto M.-G.D., Giancola G.: 'Understanding ultra wide band radio fundamentals' (Prentice-Hall, Upper Saddle River, NJ, USA, 2004)

[11] Nekoogar F.: 'Ultra-wideband communications: fundamentals and applications' (Prentice-Hall, Upper Saddle River, NJ, USA, 2005)

[12] Win M.Z., Scholtz R.A.: 'Impulse radio: how it works', *IEEE Commun. Lett.*, 1998, **2**, (2), pp. 36–38

[13] Cheng X., Guan Y.: 'Mitigation of cross-modulation interference in UWB energy detector receiver', *IEEE Commun. Lett.*, 2009, **13**, (6), pp. 375–377

[14] Urkowitz H.: 'Energy detection of unknown deterministic signals', *Proc. IEEE*, 1967, **55**, (4), pp. 523–531

[15] Humblet P., Azizoglu M.: 'On the bit error rate of lightwave systems with optical amplifiers', *J. Lightwave Technol.*, 1991, **9**, (11), pp. 1576–1582

[16] Celebi H., Arslan H.: 'Cross-modulation interference and mitigation technique for ultrawideband PPM signaling', *IEEE Trans. Veh. Technol.*, 2008, **57**, (2), pp. 847–858

[17] Cui S., Xiong F.: 'UWB system based on energy detection of derivatives of the Gaussian pulse', *Eurasip J. Wirel. Commun. Netw.*, 2011, 206, DOI: 10.1186/1687-1499-2011-206

[18] Mills R.F., Prescotte G.E.: 'A comparison of various radiometer detection models', *IEEE Trans. Aerosp. Electron. Syst.*, 1996, **32**, (1), pp. 467–474

[19] Molisch A.F., Balakrishnan K., Cassioli D., *ET AL.*: IEEE 802.15.4a channel model-final report. pp. 1–40. Available at http://www.ieee802.org/15/pub/04/15-04-0662-02-004a-channel-model-final-report-r1.pdf, accessed November 2013

[20] Arslan H.: 'Cross-modulation interference reduction for pulse-position modulation UWB signals'. IEEE 64th Vehicular Technology Conf., Montreal, Canada, September 2006, pp. 1–5

9 Appendix

We use mathematical tool MAPLE to calculate the energy distribution relationships of E_{01}, E_{02}, E_{11} and $E_{1,2}$ as follows

$$E_{01} = \int_0^{\sqrt{2}/(\alpha_0\sqrt{\pi})} [X_f]^2\,\mathrm{d}f = \int_0^{\sqrt{2}/(\alpha_0\sqrt{\pi})} \left(f^2 \mathrm{e}^{-\pi f^2 \alpha_0^2/2}\right)^2 \mathrm{d}f \tag{39}$$

$$E_{02} = \int_{\sqrt{2}/(\alpha_0\sqrt{\pi})}^{2\sqrt{2}/(\alpha_0\sqrt{\pi})} [X_f]^2\,\mathrm{d}f = \int_{\sqrt{2}/(\alpha_0\sqrt{\pi})}^{2\sqrt{2}/(\alpha_0\sqrt{\pi})} \left(f^2 \mathrm{e}^{-\pi f^2 \alpha_0^2/2}\right)^2 \mathrm{d}f \tag{40}$$

$$E_0 = \int_0^{\infty} [X_f]^2\,\mathrm{d}f = \int_0^{\infty} \left(f^2 \mathrm{e}^{-\pi f^2 \alpha_0^2/2}\right)^2 \mathrm{d}f \tag{41}$$

$$E_{11} = \int_0^{\sqrt{2}/(\alpha_0\sqrt{2})} [X_f]^2\,\mathrm{d}f = \int_0^{\sqrt{2}/(\alpha_0\sqrt{\pi})} \left(f^2 \mathrm{e}^{-\pi f^2 \alpha_1^2/2}\right)^2 \mathrm{d}f \tag{42}$$

$$E_{12} = \int_{\sqrt{2}/(\alpha_0\sqrt{\pi})}^{2\sqrt{2}/(\alpha_0\sqrt{\pi})} [X_f]^2\,\mathrm{d}f = \int_{\sqrt{2}/(\alpha_0\sqrt{\pi})}^{2\sqrt{2}/(\alpha_0\sqrt{\pi})} \left(f^2 \mathrm{e}^{-\pi f^2 \alpha_1^2/2}\right)^2 \mathrm{d}f \tag{43}$$

$$E_1 = \int_0^{\infty} [X_f]^2\,\mathrm{d}f = \int_0^{\infty} \left(f^2 \mathrm{e}^{-\pi f^2 \alpha_1^2/2}\right)^2 \mathrm{d}f \tag{44}$$

where $\sqrt{2}/(\alpha_0\sqrt{2})$ is the value of the centre frequency f_{c0} of $p_0(t)$. After substituting the values of α_0 and $\alpha_1 = 2\alpha_0$ into these equations, we obtain

$$E_{01} - E_{02} \simeq 0.451E_0 - 0.543E_0 = -0.09E_0 = -0.06E_b \simeq 0 \tag{45}$$

$$E_{01} + E_{02} \simeq 0.451E_0 + 0.543E_0 = 0.994E_0 \simeq E_0 \tag{46}$$

where $E_{01} = 0.451E_0$ and $E_{02} = 0.543E_0$ can be obtained by calculating E_{01}/E_0 and E_{02}/E_0, respectively. And E_b is the average bit energy. From (16), we know $E_0 = (2/3)E_b$ and then we use (2/3) E_b to replace E_0 in (45). The reason we round off $0.06E_b$ to 0 in (45) can be explained as follows: UWB signals are transmitted in a very low power, so $0.06E_b$ is a very small value, and when we evaluate system BER performance in terms of E_b/N_0, this $0.06E_b/N_0$ is very small compared with E_b/N_0. Therefore it is reasonable to round off $0.06E_b$ to 0. Similarly, we can obtain the relationship of E_{11} and E_{12} as

$$\begin{aligned} E_{11} - E_{12} &\simeq 0.993E_1 - 0.0068E_1 \\ &= 0.986E_1 \simeq E_1 \end{aligned} \tag{47}$$

$$\begin{aligned} E_{11} + E_{12} &\simeq 0.993E_1 + 0.0068E_1 \\ &= 0.9998E_1 \simeq E_1 \end{aligned} \tag{48}$$

These results are all verified by different values of α_0 and $\alpha_1 = 2\alpha_0$.